Albornoz-Palma, GPH.; Ortega-Sanhueza, I.; Teruel-Juanes, R.; Henríquez-Gallegos, S.; Ribes-Greus, A.; Pereira, M. (2023). Understanding the effect of lignin on the production process and characteristics of lignocellulose nanofibrils from Eucalyptus nitens. Cellulose. 30(11):6811-6831. https://doi.org/10.1007/s10570-023-05299-1

# Understanding the effect of lignin on the production process and characteristics of lignocellulose nanofibrils from *Eucalyptus nitens*

Gregory Albornoz-Palma[1,2,*], Isidora Ortega-Sanhueza[3], Roberto Teruel-Juanes[2], Sergio Henríquez-Gallegos[3], Amparo Ribes-Greus[2], Miguel Pereira[1,4]

[1]*Departamento de Ingeniería Química, Universidad de Concepción, Concepción, Chile.*
[2]*Instituto de Tecnología de Materiales (ITM), Universitat Politècnica de València (UPV), 46022 València, España.*
[3]*Facultad de Ciencias Forestales, Universidad de Concepción, Concepción, Chile.*
[4]*Centro de Excelencia en Nanotecnología (CEN), Román Díaz 532, Providencia, Santiago 7500000, Chile.*

**Abstract**

Cellulose, hemicellulose, and lignin are the main constituents of lignocellulose nanofibrils (LCNFs). The content and modification of lignin in the pulps affect the production process and characteristics of LCNFs, showing changes in their morphology, surface, rheological and dielectric behaviors. These changes are not yet clearly explained in the literature, and are even controversial, being relevant to the potential uses of this nanomaterial. This work seeks to understand the effect lignin and its oxidation have on the production process and the characteristics of LCNFs. A lower amount of lignin facilitated the LCNF production process, generating fibrils with smaller widths but larger apparent lengths. The viscosity of the suspensions increased for LCNFs with lower lignin content, due to increased flexibility, specific surface area, and surface charge of the fibrils. Finally, the LCNFs showed four dipolar relaxations, where the glass transition temperature of lignin decreased with oxidation and increased with the increase in crosslinked structures.

*Keywords: Eucalyptus nitens*, lignocellulose nanofibers, morphology, rheology, dielectric properties

## 1. Introduction

The plant cell wall is the most abundant renewable resource on the planet (Ochoa-Villarreal, 2012). Plant cells of *Eucalyptus* are mainly made up of cellulose, a linear semicrystalline polymer of anhydroglucose units with β-(1→4) bonds, hemicellulose, branched polymers formed mainly by acetylated (4-O-methylglucurono)xylan and a lower proportion of glucomannan, and lignin, an amorphous polymer chemically composed of phenylpropane units of Siringyl (S) and Guaicyl (G) type (Ek, 2009).

Plant cells are the raw material to produce lignocellulose nanofibrils (LCNFs), so the modification of their constituents affects the properties of the nanomaterial. LCNFs are flexible nano-objects with widths on the nanoscale and lengths of several microns (ISO, 2007; Albornoz-Palma, 2020b). They are produced by mechanical disintegration processes of the cell wall of the fibers in an aqueous suspension (Nechyporchuk, 2016). The size distributions tend to be non-homogeneous

*Corresponding author
Email address: gralbornoz@udec.cl

(Chinga-Carrasco, 2011), affected by the applied pretreatments (mechanical, enzymatic, or chemical) and mechanical treatments.

The rheology of LCNF suspensions is complex, as they exhibit pseudoplastic behavior, thixotropy, and yield stress (Iwamoto 2014; Nazari, 2016; Larson 2019). The variations in their behavior are related to the morphology, the surface charge, and the constituents of the fibrils.

Cellulose, hemicellulose, and lignin are polar polymers, so they become polarized under the action of an electric field. Polymers have the property of not instantly adapting to a new equilibrium situation when an external electric field is applied, giving rise to the so-called dielectric relaxations. Dielectric relaxations are manifested through a maximum of dielectric losses measured as a function of frequency and temperature (Ribes, 1986). These relaxations are caused by local and cooperative segmental motions and depend on the chemical structure and the amounts of the constituents in the LCNFs.

Dielectric relaxations are characterized by a peak in the ε'' curves and a step in the ε' curves at frequency decreases, where ε′ is the real part, and ε″ is the imaginary part of the complex dielectric permittivity (Torgovnikov, 1993; Kremer, 2012; Agrebi, 2018). Being ε' is the capacity of the material to store energy from the electric field in the material, and ε'' is the capacity of a material to absorb or dissipate energy, that is, to convert electrical energy into thermal energy (Budnikov, 2020).

The glass transition of the amorphous zones of cellulose is found at temperatures above 200°C (Back, 1982; Sun, 2007), while hemicellulose is above 150°C (Sun, 2007). The lignin of hardwood (e.g., *Eucalyptus*) exhibits a glass transition at lower temperatures, around 90°C (Sixta, 2006; Heitner, 2016).

The production of LCNFs with specific characteristics is relevant since it defines the uses of this material. Because LCNFs are produced from plant fibers of diverse origins, the morphological, rheological, and dielectric characteristics change in nanomaterials, so the origin of the raw material (physical and chemical characteristics) is critical in the production processes and features of LCNFs.

The constituents of the fibers (type and amount) affect the mechanical processes of fibrillation. The favorable effect of hemicellulose is widely known (Iwamoto, 2008; Carvalho, 2019). However, the impact of lignin has generated controversy since several articles comment that lignin hinders the fibrillation process (Ma, 2018; Gu, 2019; Jang, 2020; Yuan, 2021; Liu, 2022), while others comment that it facilitates fibrillation (Bian, 2017; Zhang, 2019; Iglesias, 2020). However, their comparisons are complex due to the multitude of raw materials, pretreatments, and treatments used.

A previous work (Albornoz-Palma, 2022) showed that native lignin hindered fibrillation by homogenization in *Pinus radiata* pulps, isolating the morphological effects. However, the removal and oxidation of lignin and the change of species (different physical and chemical properties of the fibers) would generate differences in mechanical fibrillation and properties of LCNFs. This work hypothesizes that lignin in the *Eucalyptus nitens* pulps will hinder mechanical fibrillation processes, producing LCNFs of larger size, with lower viscosity, and with differentiated dielectric properties. For this, this study aims to understand the effect that the content and oxidation of lignin from *Eucalyptus nitens* Maiden has on the production process and the morphological, rheological, and dielectric characteristics of LCNFs.

## 2. Materials and methods

**Materials:** *Eucalyptus nitens* mechanical pulp obtained through refining was used. The pulp was fractionated in a 28 mesh (707 $\mu m$), using the retained pulp on the mesh.

**Delignification process:** The fractionated pulp was subjected to a delignification process with acid chlorite with different reaction times. The reactions were carried out in pulps with a 5% (w/w) consistency, using 0.6 g of sodium chlorite at 1M and 0.2 ml of glacial acetic acid per gram of dry pulp, according to Ahlgren and Goring (1971). The reactions were carried out at 70°C in a Julabo SW22 thermal bath (under a fume hood) with intermittent agitation every 5 min. Reaction times were

1, 3, 5, and 10 h. The reagents were added at the beginning of the reaction and every 1 h of reaction time, under conditions identical to the initial charges.

**Chemical compositions of fibers:** An acid hydrolysis method was used to quantify the main constituents of plant fibers according to the method presented by Andrade et al. (2021). The extractives and ash were quantified according to T 204 cm-97 (with acetone as solvent) and T 211 cm-9, respectively.

**Morphological analysis of fibers:** The morphology of plant fibers was identified in an L&W fiber analyzer using fiber suspensions of 0.4% (w/w) consistency.

At 0.05% (p/v) fiber suspension was prepared. A drop of the suspension was deposited on a glass slide and a coverslip was placed on the samples. The fiber shapes were observed in a Carl Zeiss Primo Star microscope with scale

**Degree of polymerization:** The average degree of polymerization (DP) of cellulose was measured from the intrinsic viscosities of the cellulose dissolved in a solution of cupriethylenediamine (CED), measured according to Chakraborty et al. (2006).

**The crystallinity index (CrI):** The freeze-dried pulps with different reaction times were pressed to form 50 mg dry mass pulp pellets. The pellets were analyzed by X-ray Diffraction (XRD) in a D4 Endeavor X-ray diffractometer (Bruker AXS Gmbh, Karlsruhe, Germany) with monochromatic Cu Kα radiation ($\lambda = 0.154$ nm) at 40 kV and 20 mA, in a $2\theta$ range between 5° and 45°, with scan steps of 0.02°. The crystallinity index (CrI) was calculated according to Segal et al. (1959).

**Production of LCNF suspensions:** The pulps were refined with 50,000 revs in a PFI No 205 mill and homogenized in a Panda Plus 2000 homogenizer (GEA Niro Soavi) at a pressure of 700 bar and 0, 5, 10, and 15 passes. The consistency of the pulps in the PFI mill was 10% (w/w), while in homogenization, it was 0.5% (w/w).

**Morphological characteristics of the LCNFs:** The width distributions and average widths for the LCNFs with 15 passes through the homogenizer were determined by quantifying 1000 fibril widths from micrographs of Transmission Electron Microscopy (TEM) (Hitachi TEM) according to Albornoz-Palma et al. (2020a). The average widths of the LCNFs with 0, 5, and 10 passes through the homogenizer were determined by measuring 250 fibril widths from TEM micrographs (JEM 1200EX-II JEOL). ImageJ software was used for processing the TEM images.

The apparent length distribution and the average apparent lengths of LCNFs were measured in an S3500 Laser Diffraction Particle Size Analyzer (Microtrac Inc. USA) with a lignin refractive index of 1.61 (Li et al. 2018). Measurements were made wet with LCNF suspensions of 0.5% (w/w) consistency.

The aspect ratio of the LCNFs was calculated by dividing the average apparent length and the average width of fibrils.

The radius of gyration and the flexibility parameter of the different LCNF samples were calculated from the wormlike chain model (Mansfield and Douglas, 2008) using experimental values of average apparent lengths and widths, and intrinsic viscosity.

The specific surface area of LCNFs was calculated considering a cylindrical configuration and homogeneous distribution from the average apparent lengths and widths, considering a fibril density of 1.5 g/cm$^3$ (Ansari, 2016)

**The viscosity of LCNF suspensions and the intrinsic viscosity of LCNFs:** A rotational viscometer (Fungilab Premium-L, USA) was used at 25°C and 73.38 s$^{-1}$, with suspensions of LCNFs from 0.02% to 0.5% (w/w) of consistency. The concentration range between 0.02% and 0.08% was used to determine the intrinsic viscosity.

**Lignin nanoparticles:** The quantification of the lignin nanoparticles was carried out according to Albornoz-Palma et al. (2022).

**ζ-potential of LCNF suspension:** Particle Metrix equipment (Stabino) was used to measure the ζ-potential of LCNFs in suspensions of 0.05% (w/w) consistency and pH of 4.7± 0.3. The method used was the Transmission Potential method.

**Formation of nanopapers:** LCNF nanopapers with a grammage of 800 g/m$^2$ were produced. The 0.5% (g/g) LCNF suspensions were concentrated up to 15% (g/g) by vacuum filtration, using 0.45µm pore diameter membranes, followed by filtration in a Buchner funnel with a 6 cm diameter fritted disk. The nanopapers were pressed and dried in a vacuum oven for 7 days.

**Fourier-Transform Infrared Spectroscopy (FTIR):** FTIR spectroscopy measurements of the LCNF nanopapers were performed, in an Agilent Cary 630 FTIR spectrometer (Mettler Toledo, USA) in the attenuated total reflectance mode (ATR). The spectra were measured in the wavelength range from 4000 to 500 cm$^{-1}$ with a 4 cm$^{-1}$ resolution and an average of 64 scans. Spectra were area normalized and compared (principal component analysis) in The Unscrambler X program.

**Thermogravimetric analysis (TGA):** Thermal decomposition of LCNF nanopapers tests were performed in a TGA 851 analyzer (Mettler Toledo, USA). Samples of 3 to 5 mg were introduced into 70 µL alumina capsules. The temperature range was from 25°C to 600°C at a rate of 10°C/min in an oxidative atmosphere (50 mL/min).

**Differential Scanning Calorimetry (DSC):** The glass transition temperatures of lignin were determined in a DSC 822e (Mettler Toledo, USA) equipped with a cooling system. LCNF nanopapers samples of 3 and 5 mg were placed in 40 µL aluminum crucibles. The analysis method consisted of different consecutive heating/cooling/heating segments between -10°C and 200°C with a heating/cooling rate of 10°C/min. The tests were carried out under an inert atmosphere of $N_2$ at 50 mL/min flow.

**Dielectric Thermal Analysis (DETA):** For dielectric measurements of LCNF nanopaper samples, a frequency analyzer in conjunction with an active cell (Concept 40, Novocontrol Technologies BmgH & Co. Kc, Hundsangen, Germany) was used. The frequency range was from $10^{-2}$ to $10^7$ Hz, and the temperature range was from -120 to 180°C, controlled by the Quatro system (Novocontrol Technologies, Germany). Spectra were obtained under isothermal conditions by increasing steps of 10°C.

The relaxations of the LCNFs were identified by the spectra of ε". The Charlesworth deconvolution method adding Havriliak-Negami (HN) relaxation functions was used (Havriliak, 1966; Havriliak, 1967; Charlesworth, 1993), obtaining the maximum relaxation times ($\tau_{max,j}$) for each temperature and relaxations from Equation 1 and Equation 2.

$$\varepsilon''(f) - \varepsilon_\infty = \sum_j Im\left(\frac{\Delta\varepsilon}{\left(1 + \left(if\tau_{HN,j}\right)^{a_j}\right)^{b_j}}\right) \quad (1)$$

$$\tau_{max,j} = \tau_{HN,j}\left(\frac{\sin\left(\frac{b_j(a_j)\pi}{2(b_j+1)}\right)}{\sin\left(\frac{(a_j)\pi}{2(b_j+1)}\right)}\right)^{\frac{1}{a_j}} \quad (2)$$

where $\varepsilon_\infty$ is the high frequency limit value of the permittivity, $\Delta\varepsilon$ is the relaxation strength, f is the frequency, $\tau_{HN,j}$ is the Havriliak-Negami relaxation time of the $j$-relaxation, $a_j$ and $b_j$ are parameters associated to the width and asymmetry of $j$-relaxation.

The dipolar relaxations were fitted to the Arrhenius equation:

$$f_{max,j} = \frac{1}{\tau_{max,j}} = f_{0,j}\exp\left(-\frac{E_{a,j}}{RT}\right) \quad (3)$$

where $f_{max,j}$ is the maximum frequency of $j$-relaxation, $f_{0,j}$ is the pre-exponential factor, $E_{a,j}$ is the activation energy of $j$-relaxation, R is the gas constant, and T is the temperature (K).

The dynamic glass transition relaxation was fitted using the Vogel-Fulcher-Tammann-Hesse equation (Fulcher, 1925; Badia, 2021):

$$f_{max,j} = f_{0,j} \exp\left(-\frac{D_{0.j} T_{v,j}}{T - T_{v,j}}\right) \quad (4)$$

where $D_{0.j}$ is a fragility or strength parameter, and $T_{v,j}$ is the Vogel temperature (K).

**Data analysis:** The statistical analysis of the data was performed with the Statgraphics Centurion XVIII program (Albornoz-Palma, 2022).

## 3. Results and discussion

**Pulp characterization:** The acid chlorite delignification process selectively removed lignin, since the percentages of cellulose (49.4±0.2%) and hemicellulose (25.4±0.2%) in the native and delignified pulp did not vary (Figure 1a). The characterization of the fibrils showed 0.95±0.02% and 0.28±0.01% of extractives and ashes, respectively. Furthermore, lignin removal was 21%, 51%, 64%, and 71% for 1, 3, 5, and 10 h reaction time, respectively (concerning lignin in Eucalyptus-0h). Lignin removal using acid chlorite in *Eucalyptus nitens* followed the same trend as for *Pinus radiata* (Figure S1 Supplementary material). The percentages of the constituents of the *Eucalyptus nitens* fibers agree with those reported in the literature. (Ek, 2009; Antes, 2015; Wentzel, 2019).

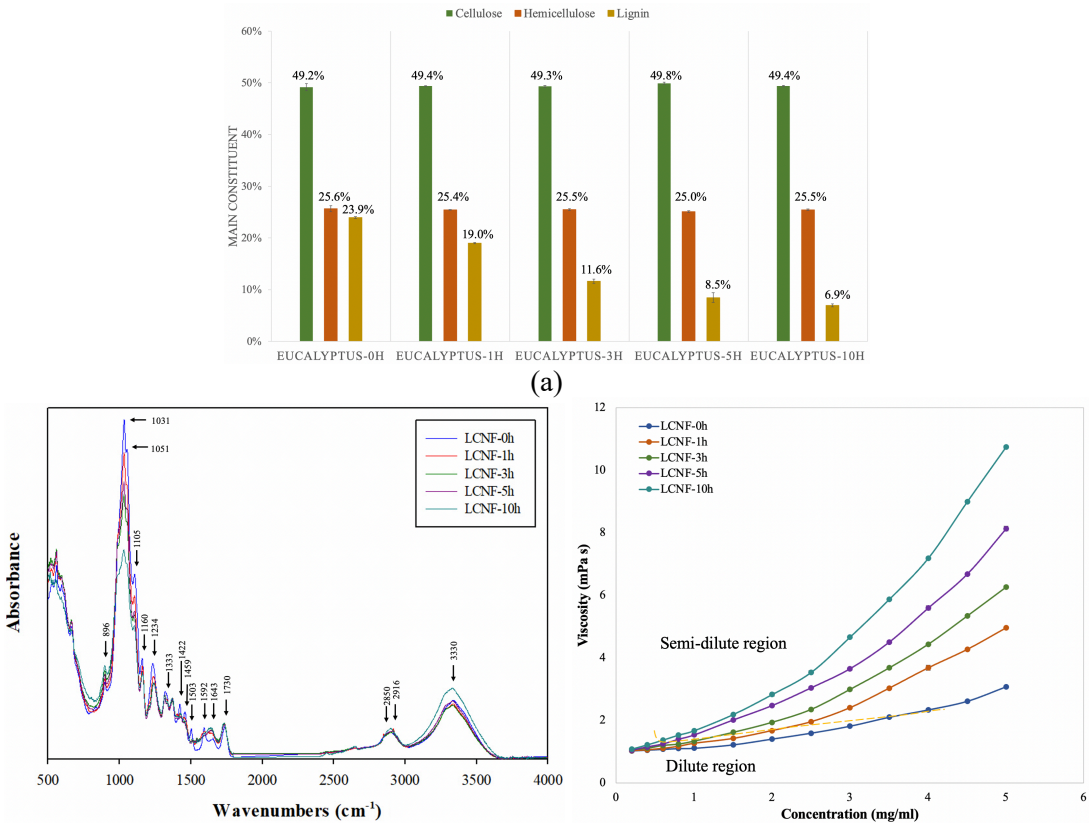


**Figure 1.** (a) Chemical composition of native and bleached mechanical *Eucalyptus* pulps, (b) FTIR-ATR spectrum of LCNFs with native and oxidized lignin, and (c) variation in the viscosity according to concentration for LCNFs from *Eucalyptus nitens*.

The morphological characterization of the fibers is shown in Table 1. The delignification process did not generate significant differences in length, diameter, and the number of fibers/mg between all samples (with 95% confidence). The width and length of the fibers are higher than that reported in the literature of approximately 20 µm y 1 mm, respectively (Ek, 2009; Morais, 2019). This indicates that in the fiber production process, the chips did not disintegrate into fibers, but a non-homogenous material containing fibers, fiber aggregates, and chip fragments was produced, wherein the largest size fraction, used in this work, are mostly fiber aggregates and chip fragments (Figure S2, Supplementary material). On the other hand, a percentage of fines is removed during the delignification process due to fibers washing. The crystallinity index did not show significant differences (with 95% confidence) up to 10 h of reaction, with a value similar to those reported in the literature (Lekha, 2016; Wentzel, 2019). The crystallinity index increases at 10 h due to oxidative reactions in the amorphous zone of the cellulose. The degree of polymerization should not have changed with the delignification process, so it is considered 1643 for all samples (Malešič, 2021). A similar value was reported for *Eucalyptus nitens* (Andrade, 2021).

**Table 1.** Morphological characteristics of *Eucalyptus* pulps.

| Properties | Eucalyptus-0h | Eucalyptus-1h | Eucalyptus-3h | Eucalyptus-5h | Eucalyptus-10h |
|---|---|---|---|---|---|
| Average length (mm) | 1.4±0.1 | 1.4±0.1 | 1.4±0.1 | 1.5±0.1 | 1.3±0.1 |
| Average width ($\mu$m) | 41.2±0.1 | 40.4±0.9 | 40.9±0.2 | 41.2±1.2 | 40.2±0.2 |
| Crystallinity index (%) | 64.9±0.2 | 65.5±0.5 | 65.1±1.0 | 65.9±0.1 | 69.0±0.6 |
| Fines (%) | 48.3±0.8 | 49.3±0.2 | 47.6±0.3 | 41.2±0.9 | 39.3±0.3 |
| Number of fibers/mg (N°/mg) | 126±17 | 122±19 | 124±5 | 121±10 | 121±2 |
| Degree of polymerization | | | 1643 | | |

**Chemical characteristics of LCNFs.** Lignin is a complex polymer composed of monomers linked by ether and carbon-carbon bonds in an irregular pattern (Nunes, 2010). The lignin in eucalyptus fibers is mainly composed of guaiacyl (G) and syringyl (S) units (Ek, 2009). The S/G ratio is approximately 3.7 (Rencoret, 2007; Antes, 2015).

Delignification with acid chlorite (chlorine dioxide) is a highly selective oxidative process that attacks the aromatic rings of lignin, producing muconic acid ester, maleic acid, C5-acid, and quinone (Collings, 1978; Lemeune, 2004; Tarvo, 2010;). Furthermore, oxidative processes are generated in the aliphatic chain of lignin, where the methoxy or methylene group is oxidized to the carbonyl group (Kolar, 1983).

The changes in the surface chemical characteristics of the LCNFs are shown in the FTIR-ATR absorption spectra in Figure 1b. All the spectra showed the same bands with differences in absorbance. LCNF-0h, LCNF-1h, LCNF-3h, LCNF-5h, and LCNF-10h are LCNFs with 15 passes through the homogenizer and different reaction times (0, 1, 3, 5, and 10 h).

The increase in the 3330 $cm^{-1}$ band, corresponding to the -OH stretching (Lehto, 2018), indicates an increase in the -OH groups on the surface of the fibrils. This is caused by a higher exposure of cellulose on the surface (Kumagai, 2018), which has a higher amount of -OH groups (Ben, 2018). The 2916 and 2850 $cm^{-1}$ peaks, associated with the C–H stretch of methyl and methylene groups (sp3) (Stark, 2016), showed an increase in LCNF-10h. This increase may be due to a higher presence of methyl groups on the surface of the fibrils caused by a higher exposure of cellulose.

The 1730 $cm^{-1}$ peak corresponds to the C=O stretching of the unconjugated ketone, carboxyl, and ester groups (Stark, 2016). This increases slightly for LCNFs with lower lignin content, indicating higher oxidation of the lignin ring (formation of C5-acid, maleic acid, and muconic acid) and the aliphatic chains. An increase in the 1643 $cm^{-1}$ peak is observed, related to the C=O stretching of aryl

ketone and conjugated C=C stretch (Hergert, 1960; Chen, 2018), due to the rupture of the benzene rings.

The 1592 and 1503 $cm^{-1}$ peaks, corresponding to the aromatic skeletal vibration (Lisperguer, 2009; Awal, 2011), and the 1333 $cm^{-1}$ peak, corresponding to aryl ring breathing with C–O stretch (Stark, 2016) are higher for LCNF-0h, due to the higher presence of aromatic rings.

An increase in the 1422 and 1459 $cm^{-1}$ peaks was observed for the LCNFs with lower lignin content, corresponding to the $CH_2$ deformation stretching in lignin and xylan (Lehto, 2018). The 1422 $cm^{-1}$ peak is also related to the O-$CH_3$ and C-H deformation asymmetric (Stark, 2016). This decrease indicates an increase in lignin oxidation.

LCNFs with lower lignin content show a decrease in the 1234 and 1160 $cm^{-1}$ peaks, related to the C–O stretching of the ether group (Lehto, 2018). This indicates the rupture of the β-O-4 ether bonds. In 1105, 1051, and 1031 $cm^{-1}$ peaks, caused by the vibrations of C═O bonds in primary and secondary alcohol, a progressive decrease is observed for the delignified LCNFs, indicating a lower number of aliphatic and phenolic -OH groups.

Finally, the peak at 896 $cm^{-1}$ is attributed to CH out of plane glucose ring in cellulose and hemicellulose and for guaiacyl rings in lignin (Lehto, 2018), being higher for oxidized LCNFs, indicating the higher exposure of cellulose.

The FTIR-ATR spectra showed that the delignified LCNFs present a greater exposure of the cellulose on their surface. Lignin in delignified LCNFs showed higher oxidation, with fewer aliphatic and phenolic hydroxyl groups, more ester, ketone, and carboxylic acid groups than native lignin, and increased cleavage of β-O-4 ether bonds.

**Morphological characteristics of LCNFs.** LCNFs are high aspect ratio nano-objects, as seen in Table 1 and Figure S3, Supplementary material. The effect that the homogenization process and the mechanical pretreatment by refining have on the LCNFs with different lignin content is shown in Table 2.

**Table 2.** Morphological characterization of LCNFs with different numbers of passes through the homogenizer and lignin content.

| Raw materials (lignin content) | Passes | Average Width (nm) | Variation of width[(a)] (%) | Apparent average length ($\mu m$) | Variation of apparent length[(b)] (%) | ζ-potential[(c)] | Aspect ratio | Intrinsic viscosity (ml/g) | Lignin nanoparticle[(d)] (% g/g) |
|---|---|---|---|---|---|---|---|---|---|
| Eucalyptus-0h (23.9%) | 0 | 145.8 | - | 8.8 | - | -23.3 | 60 | 109 | 2.0 |
| | 5 | 92.4 | 37 | 7.6 | 14 | -22.6 | 82 | 156 | 2.1 |
| | 10 | 67.1 | 54 | 6.4 | 27 | -22.1 | 95 | 194 | 2.1 |
| | 15 | 48.5 | 67 | 5.5 | 38 | -24.0 | 113 | 273 | 2.6 |
| Eucalyptus-1h (19.0%) | 0 | 128.1 | - | 10.7 | - | -27.1 | 84 | 169 | 6.0 |
| | 5 | 78.6 | 39 | 8.6 | 20 | -28.1 | 109 | 256 | 9.3 |
| | 10 | 55.4 | 57 | 7.7 | 28 | -28.3 | 139 | 354 | 9.6 |
| | 15 | 42.7 | 67 | 6.5 | 39 | -28.9 | 152 | 450 | 10.0 |
| Eucalyptus-3h (11.6%) | 0 | 102.0 | - | 13.1 | - | -28.2 | 128 | 301 | 9.1 |
| | 5 | 75.3 | 26 | 10.9 | 17 | -28.4 | 145 | 385 | 9.3 |
| | 10 | 50.6 | 50 | 9.2 | 30 | -28.5 | 182 | 569 | 9.8 |
| | 15 | 35.1 | 66 | 7.8 | 40 | -28.3 | 222 | 809 | 10.0 |
| Eucalyptus-5h (8.5%) | 0 | 93.1 | - | 14.2 | - | -28.8 | 153 | 426 | 9.2 |
| | 5 | 64.5 | 31 | 11.1 | 22 | -28.1 | 172 | 602 | 9.8 |
| | 10 | 40.1 | 57 | 9.4 | 34 | -26.1 | 234 | 838 | 10.7 |
| | 15 | 33.0 | 65 | 9.0 | 37 | -25.4 | 273 | 1072 | 11.8 |
| Eucalyptus-10h (6.9%) | 0 | 79.2 | - | 15.2 | - | -38.6 | 192 | 562 | 9.0 |
| | 5 | 51.9 | 34 | 11.7 | 23 | -34.1 | 225 | 828 | 10.7 |
| | 10 | 35.4 | 55 | 9.7 | 36 | -34.2 | 274 | 1065 | 11.2 |
| | 15 | 25.1 | 68 | 9.0 | 41 | -32.5 | 359 | 1710 | 11.9 |

[(a)] Normalized to the average width of 0 passes through the homogenizer for each raw material.
[(b)] Normalized to the apparent average length of 0 passes through the homogenizer for each raw material.
[(c)] pH of 4.7 ± 0.3.
[(d)] Based on total lignin.

The mechanical pretreatment by refining generates a decrease in the average widths and an increase in the average apparent lengths of the fibrils (0 passes) with lower lignin content. In addition, there is an increase in the ζ-potential (absolute value), indicating an increase in lignin oxidation. Mechanical pretreatment is a disintegration process by shear forces on the fiber surface. The rise in lignin oxidation due to the delignification process and the exposure of cellulose and hemicellulose generates an increase in the polar groups and, therefore, in the polarity of the LCNFs (Gindl-Altmutter, 2015). The higher amount of these groups favor water retention in the fibrils (Pejic, 2008), improving fibril-solvent interactions and causing their swelling. This swelling favors the longitudinal disintegration of fibers, allowing shear forces to predominantly disintegrate the cell wall, while less swelling increases the rupture of fibers.

For each raw material, the average width and apparent length of the LCNFs tend to decrease with the homogenization process. The longitudinal disintegration is the most affected (higher variation of width), which increases the aspect ratio. This is because the homogenization process generates the disintegration of the fibrils using the mechanism of impact and shear force mainly (surface mechanisms) (Lee, 2014; Costa, 2018).

For all LCNF samples with the same number of passes through the homogenizer, the variation of width and apparent length don´t change significantly. In the case of LCNF-3h and 0 and 5 passes through the homogenizer, a slight drop in width variation is observed. This could be due to the high delignification generated in this sample, which indicates a difficulty in fibrillation in the first stages of homogenization. The ζ-potential doesn´t show changes between the LCNFs with 1 and 3 h of reaction time, so the differences in the variation of width are due to the smaller lignin content. The production of nanofibrils from the pulp with 10 h of reaction time does not show differences in the variation of width and apparent length, for all the passes, despite showing an increase in ζ-potential (absolute value) and cellulose crystallinity index (Table 1 and Table 2), caused by the rupture of part of the amorphous zones of the cellulose. This indicates that the content and degree of lignin oxidation do not affect the homogenization process.

The intrinsic viscosity of LCNFs is directly related to the morphology of the fibrils, specifically with the aspect ratio (Albornoz-Palma, 2020a; Bastida, 2022). The intrinsic viscosity increases with the mechanical processes of refining and homogenization due to the decrease in the size of the fibrils and the increase in the nanofibrillar population that generates an increase in the hydrodynamic volume of the fibrils/g fibrils.

Lignin nanoparticles produced during mechanical fibrillation processes increase with homogenization and the degree of oxidation of lignin. This is due to the decrease in the molecular weight of lignin and the increase in the disintegration of fibril (Meng, 2017; Jiang, 2018; Albornoz-Palma, 2022)

**Morphological and rheological characteristics of LCNFs with 15 passes through the homogenizer.** The characterization of LCNFs is complex, since mechanical processes produce wide size distributions (Chinga-Carrasco, 2011), caused by entanglements and flocs that the fibrils in suspension.

To understand the effects that lignin (amount and degree of oxidation) has on the characteristics of the fibrils, more specific analyzes were carried out for the LCNFs with 15 passes through the homogenizer (LCNF-0h, LCNF-1h, LCNF-3h, LCNF-5h, and LCNF-10h).

The distribution of width and apparent length are shown in Figure 2. The width distribution shows that as the lignin content decreases (Figure 2a-e), the distributions tend to be more homogeneous and shift towards smaller widths values, increasing the nanofibrillar yield. The statistical parameters are shown in Table 3, where the average width, the standard deviation of the sample, and the coefficient of variation decreased for lower lignin content. The nanofibrillar yield (fibrils with widths lower than 100 nm) increases from 93% for LCNF-0h to 94, 96, 97, and 99% for LCNF-1h, LCNF-3h, LCNF-5h, and LCNF-10h respectively. On the other hand, the distributions of apparent length show the opposite trend (Figure 2f-j), moving towards higher values of lengths. The

statistical parameters of the distributions show an increase in the apparent length and standard deviation of the samples for the LCNFs with lower lignin content. However, the coefficient of variation did not change, indicating that the heterogeneity of the distribution concerning the mean did not change. This show that regardless of the content and degree of oxidation of lignin, the homogenization process does not affect the heterogeneity of the distribution of apparent length. The microfibrillar yield (fibrils with apparent length lower than 1 μm) decreases from 10.8% for LCNF-0h to 8.5, 8.3, 4.5, and 4.3% for LCNF-1h, LCNF-3h, LCNF-5h, and LCNF-10h respectively.

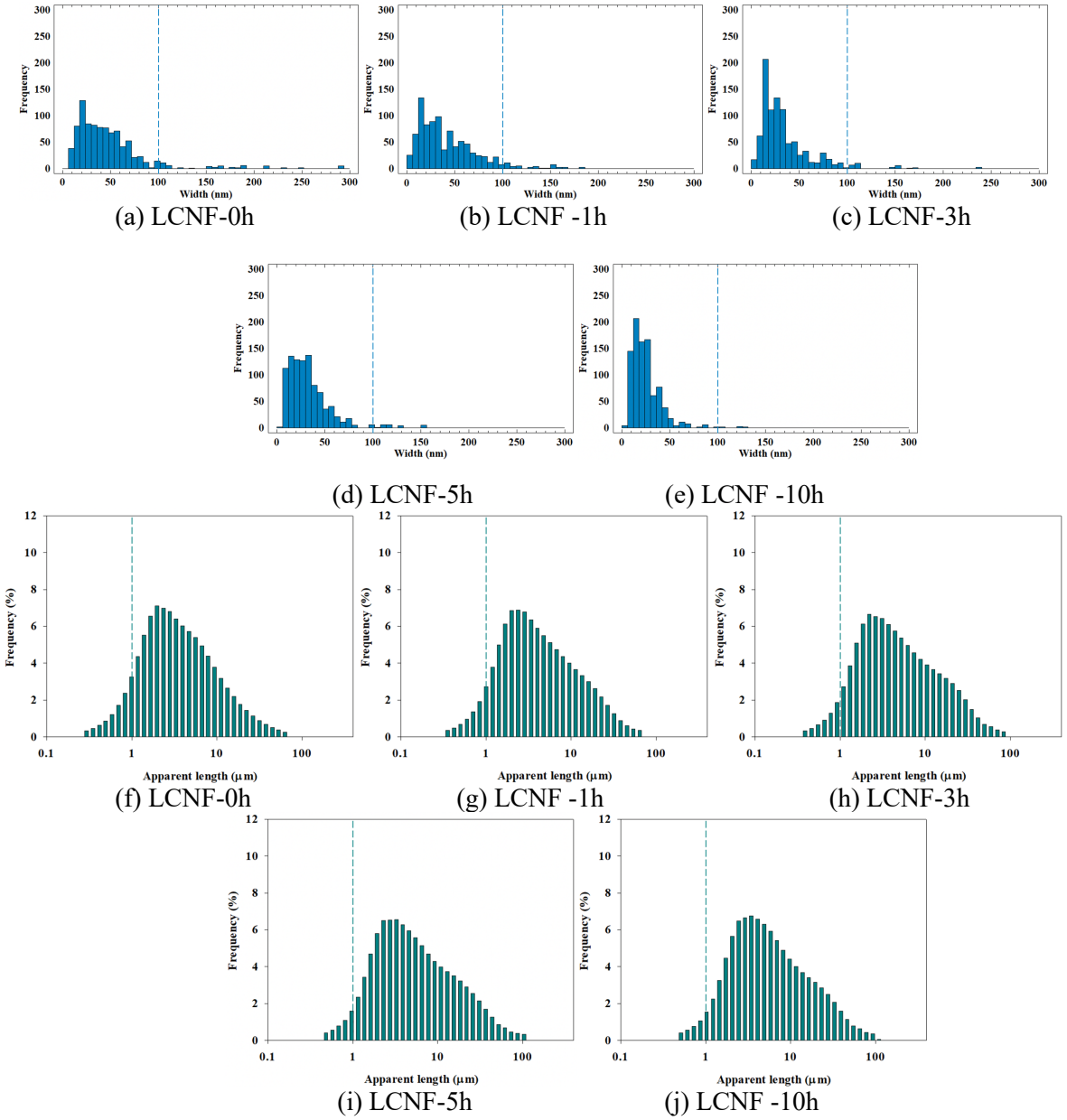


(a) LCNF-0h (b) LCNF -1h (c) LCNF-3h

(d) LCNF-5h (e) LCNF -10h

(f) LCNF-0h (g) LCNF -1h (h) LCNF-3h

(i) LCNF-5h (j) LCNF -10h

**Figure 2**. (a-e) Width distributions, and (f-j) apparent length distributions of LCNFs from *Eucalyptus pulps*.

To compare the morphology of the fibrils, the radius of gyration of a fibril was determined (a parameter that characterizes the size of particles of any shape (Jones, 2008)). Table 3 shows that the

radius of gyration increases for LCNFs with lower lignin content. Although the width of the fibrils decreases for the LCNFs with lower lignin content, their mass distribution was found further from the center, due to the increase in the apparent length despite having a lower average mass by fibrils). This indicates that the mechanical pretreatment is highly selective in the longitudinal disintegration over the transverse disintegration of the fiber of *Eucalyptus nitens*.

The decrease in the size of the fibrils for LCNFs with lower lignin content produced an increase in the specific surface area and the intrinsic viscosity (Table 2 y Table 3). On the other hand, the flexibility of the fibrils and the critical concentration decrease for LCNFs with lower lignin content, due to the reduction of the cementing capacity of the lignin (caused by depolymerization and content of lignin) and the increase in the aspect ratio. These increases favor the formation of entanglements and flocs, displacing the diluted region to lower concentrations (Figure 1c and Table 3).

Analyzing the semi-dilute region in Figure 1c (above the critical concentration), a progressive increase in viscosity is observed for all LCNFs. This is due to the formation of larger flocs with increasing concentration, caused by the higher probability of contact between the fibrils. However, the resistance to flow increases for fibrils with a lower lignin content (for any concentration). This indicates that the flocs that form for the LCNFs with lower lignin content are larger, stronger, and more hydrated. This is due to the increase in the specific surface area, the surface charge, and the polar groups in the fibrils, caused by the oxidation of lignin and exposure of cellulose.

When comparing the viscosities measured in the semi-dilute region of LCNFs with the same delignification (5h reaction time) and production process for different raw materials: *Pinus radiata* (LCNFs-5hP) and *Eucalyptus nitens* (LCNFs-5hE), the viscosities of the LCNF-5hP sample are higher (Figure S4, Supplementary material). This is due to the smaller size of the fibrils of *Pinus radiata*, which generates larger, stronger, and hydrated flocs, despite having similar ζ-potentials. This shows that a lower lignin content in *Eucalyptus nitens* pulps produces fibrils with larger morphologies and lower viscosities than *Pinus radiata* pulps, with similar ζ-potentials and degrees of delignification (Figure S1, Supplementary material).

**Table 3.** Morphological and rheological characterization of LCNFs with 15 passes through the homogenizer and different lignin content.

| Sample (lignin content) | Average width ($nm$) | S.D. of the sample [a] ($nm$)/Coefficient of variation (%) | Average apparent length ($\mu m$) | S.D. of the sample ($\mu m$)/Coefficient of variation (%) | Radius of gyration[b] ($\mu m$) | Specific surface area[c] ($m^2/g$) | Flexibility parameter[b] | Critical concentration[d] (mg/ml) |
|---|---|---|---|---|---|---|---|---|
| LCNF-0h (23.9%) | 48.5±0.3 | 13.8/29 | 5.5±0.1 | 2.76/50 | 1.36 | 55 | 0.53 | 3.66 |
| LCNF-1h (19.0%) | 42.7±0.6 | 11.8/28 | 6.5±0.1 | 3.25/50 | 1.57 | 62 | 0.49 | 2.22 |
| LCNF-3h (11.6%) | 35.1±0.3 | 9.0/26 | 7.8±0.1 | 3.99/51 | 1.84 | 76 | 0.42 | 1.24 |
| LCNF-5h (8.5%) | 33.0±0.2 | 8.3/25 | 9.0±0.1 | 4.46/50 | 2.10 | 81 | 0.39 | 0.93 |
| LCNF-10h (6.9%) | 25.1±0.6 | 5.8/23 | 9.0±0.1 | 4.49/50 | 2.06 | 106 | 0.35 | 0.58 |

[a]Normal distribution by the central limit theorem.
[b]Wormlike chain model (Mansfield y Douglas, 2008)
[c] Considering the density of the LCNFs as 1.5 g/cm$^3$ (Ansari, 2016)
[d]Calculated by equation $\eta_{sp} = ac^n$ (Murali Krishnan, 2010)

**Thermogravimetric and differential scanning calorimetry analysis of LCNFs.** The thermal stability of the LCNFs was evaluated by thermogravimetric analysis (TGA). Figure 3 shows the TGA and DTG spectra of the different LCNFs. The degradation trend agrees with that reported in the literature for cellulosic nanomaterials (Zeng, 2016). Figure 3 and Table 4 show that the degradation onset temperature ($T_{onset}$) does not change with the content or degree of oxidation of lignin (Iglesias, 2020).

The main constituents of LCNFs are cellulose, hemicellulose, and lignin. Each of them has different speeds and degradation temperatures. Cellulose and hemicellulose decompose in a short range (above 315°C for cellulose and 190°C for hemicellulose approximately), and lignin decomposition occurs over a wide temperature range, above 210°C approximately (Yang, 2007; Dorez, 2014; Cao, 2019). Figure 3 and Table 4 show three stages (three peaks) in the degradation for all samples. The first stage (Peak 1) is associated with the loss of moisture in the samples between 47 and 114°C, with moisture content in the nanopapers lower than 5.1% for all samples, corresponding to retained or bound water. The end set temperature ($T_{endset}$) does not vary significantly with the content and degree of oxidation of lignin, except for LCNF-10h, where a greater exposure of cellulose facilitates the formation of hydrogen bonds between the fibrils and the water, increasing the evaporation temperature.

In the second and third stages (Peak 2 and 3), above 250°C, degradation is generated mainly by the thermal decomposition of hemicellulose and lignin, and the start of cellulose degradation at Peak 2, and mainly due to the degradation of cellulose and lignin in Peak 3. The temperatures of maximum degradation in both stages ($T_{peak\ 2}$ and $T_{peak\ 3}$) showed a decrease with the oxidation of lignin (LCNF-1h) and then an increase with decreasing oxidized lignin content in the samples. This can be explained due to the bond breaking and decrease in the molecular weight of lignin due to the delignification process, followed by an increase in condensed and crosslinked structures (Meng, 2017), which have a higher bond breaking temperature and degradation (Brebu, 2010).

Finally, the amount of ashes in the sample was approximately 0.3% (w/w) of the original mass of the samples, above 500°C, which agrees with what was reported for *Eucalyptus nitens* pulps.

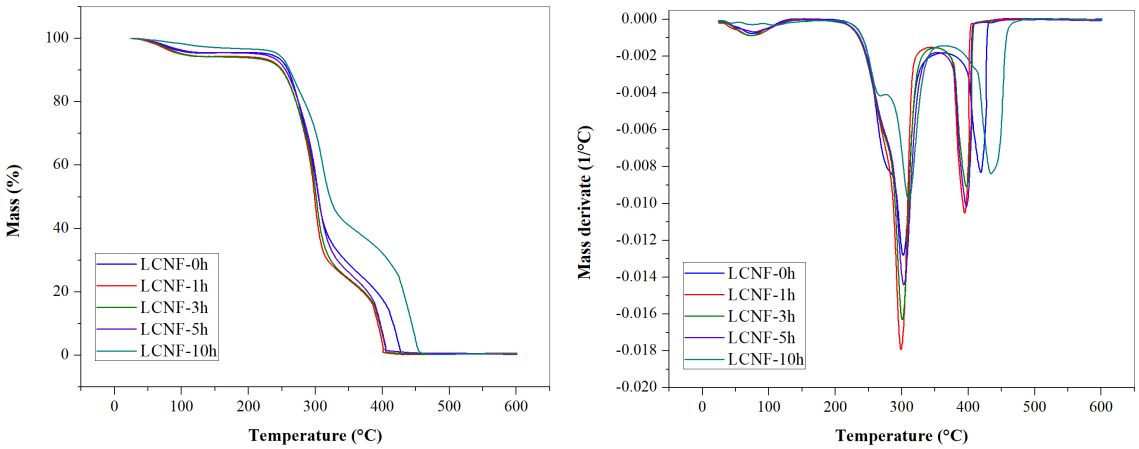


(a) (b)

**Figure 3.** (a) TGA and (b) DTG spectra of LCNFs from *Eucalyptus nitens*.

The glass transition temperature of lignin (Tg) is influenced by several factors, such as the presence of rigid phenolic groups in the main chain and crosslinked structures, the number of bonds, the molecular weight, and the type of lignin, among others (Heitner, 2016; Börcsök, 2021). Due to the configuration of lignin in hardwoods (presence of S-type lignin), it has a lower proportion of condensed bonds and an increase in the number of β-O-4 ether bonds, so it is thought that lignin is more linear and less branched than softwood lignin (Ek, 2009).

When studying the glass transitions by differential scanning calorimetry (DSC) analysis, a glass transition associated with lignin was observed. The results are shown in Table 4. The glass transition temperature decreases with the oxidation of lignin due to the decrease in its molecular weight, facilitating the motion of lignin macromolecules. On the other hand, the heat capacity difference (ΔCp) at Tg decreases with lignin oxidation due to the increase in crosslink density (Heitner, 2016).

For the LCNF-3h sample, an increase in Tg and ΔCp is observed, which indicates a decrease in the crosslinked structures. This can be explained by the high level of delignification generated between 1 and 3 h of reaction time, corresponding to an increase of at least 30% over the deslignification obtained with the other reaction times. This level of deligninification generated the elimination of a large part of the lignin (39% concerning the lignin in LCNF-1h), where an important part of the crosslinked structures was removed. Now, G-type lignin is less reactive than S-type lignin, since the β-O-4 bonds found in S-type lignin are more easily cleaved than those in G-type lignin (Muraleedharan, 2018), so the S/G ratio must have decreased (Meng, 2018). G-type lignin is less dynamic and has lower thermal mobility than S-type lignin due to the lower amount of methoxy groups and its more crosslinked structure, so its glass transition temperature is higher (Sixta 2006; Nair, 2014; Vural, 2018).

For LCNF-5h and LCNF-10h, the ΔCp, and Tg of LCNF-10h increased, due to the increase in crosslinked or condensed structures produced by lignin oxidation and the decrease in the S/G ratio. However, for LCNF-5h, the Tg decreased due to the high level of delignification (27% concerning lignin in LCNF-3h) that generated a decrease in molecular weight and an increase in the polar groups in lignin (absorption without difference of the carbonyl and carboxylic groups in the FTIR-ATR spectra, Figure 1b), facilitating the motion of lignin.

**Table 4.** Moisture and peaks of the thermal decomposition of LCNF nanopapers, and glass transition temperature and heat capacity difference of lignin in LCNFs from Eucalyptus *nitens*.

| | Moisture | | | Degradation | | | Tg (°C) | ΔCp (J/gK) |
|---|---|---|---|---|---|---|---|---|
| Peak | Peak 1 | | | - | Peak 2 | Peak 3 | | |
| Sample | $T_{onset*}$ (°C) | $T_{endset}$ (°C) | Moisture (%) | $T_{onset}$ (°C)[(a)] | $T_{peak\ 2}$ (°C) | $T_{peak\ 3}$ (°C) | | |
| LCNF-0h | 49.5 | 99.1 | 4.3 | 258.3±0.4 | 302.1±0.2 | 418.9±1.8 | 80±3 | 0.240 |
| LCNF-1h | 47.4 | 101.3 | 4.9 | 253.2±0.3 | 298.6±0.3 | 394.6±3.8 | 71±1 | 0.174 |
| LCNF-3h | 47.7 | 98.8 | 5.1 | 252.3±1.2 | 300.7±1.1 | 397.3±2.1 | 79±1 | 0.212 |
| LCNF-5h | 49.5 | 103.9 | 4.5 | 254.7±0.6 | 303.4±1.0 | 398.1±1.2 | 74±2 | 0.183 |
| LCNF-10h | 52.0 | 113.2 | 4.1 | 258.0±0.2 | 309.6±1.0 | 434.9±1.2 | 104±1 | 0.068 |

[(a)]Corresponding to a degradation of 5%

**Dielectric characteristics of LCNFs.** The dielectric spectra of the LCNFs are shown in Figure 4a-e. The spectra of ε' and ε'' as a function of frequency and temperature showed all the dielectric relaxations. LCNFs are constituted of amorphous polar polymers (hemicellulose and lignin) and semi-crystalline (cellulose). The dipolar relaxations showed by LCNFs can be dynamic relaxations of the glass transition (α) caused by cooperative segmental motions, and secondary relaxations (β and γ) that are related to the change in mobility of some units or groups in an amorphous phase (Ioelovich, 2016).

Figure 4a-e shows four dipolar relaxations which have been assigned as $\gamma_2$-, $\gamma_1$-, $\alpha_2$-, and $\alpha_1$-relaxations, named from low to high temperature. The electrical conduction phenomena in the ε'' curves were observed, with an exponential increase in these (Kremer, 2012). At high temperature and low frequency, a relaxation is observed that can be attributed to interfacial polarization is known as the Maxwell-Wagner-Sillars (MWS) effect, due to the differences in the dielectric properties of the components of LCNFs at the interfaces of the nanomaterials. (Agrebi, 2018; Torgovnikov, 1993).

To study the dipolar relaxations, the maximum relaxation times at each temperature were determined. Secondary relaxations are characterized by following the Arrhenius equation, while dynamic glass transition relaxations follow the Vogel-Fulcher-Tammann-Hesse (VFTH) equation. This is due to an increase in the mobility of the polymeric chains, giving rise to a rearrangement,

where the permanent dipoles attached to the polymeric chain are free to orient themselves in the direction of the field, showing a curved trend in the Arrhenius map.

The dipolar relaxations identified in the ε" spectra for the LCNFs are shown in Figure 4f-j. The activation energies of the secondary relaxations are shown in Table 5.

$\gamma_1$-relaxation and $\gamma_2$-relaxation that occur at low temperatures are associated with the mobility of the -OH groups of lignin and the -OH and -$CH_2$OH groups of cellulose and hemicellulose, whose activation energy values agree with those presented in the literature (Ioelovich, 2016; Roig, 2017; Vural, 2018). The activation energies of $\gamma_1$-relaxation and $\gamma_2$-relaxation increase with oxidation and the decrease in the lignin content of fibrils. This increase is due to the rise in the condensed structures in the lignin, which can hinder the molecular motion of the hemicellulose side groups. The decrease in activation energy in $\gamma_1$-relaxation for LCNF-3h could be due to the decline in part of the crosslinked lignin, facilitating the molecular motion of the -OH groups.

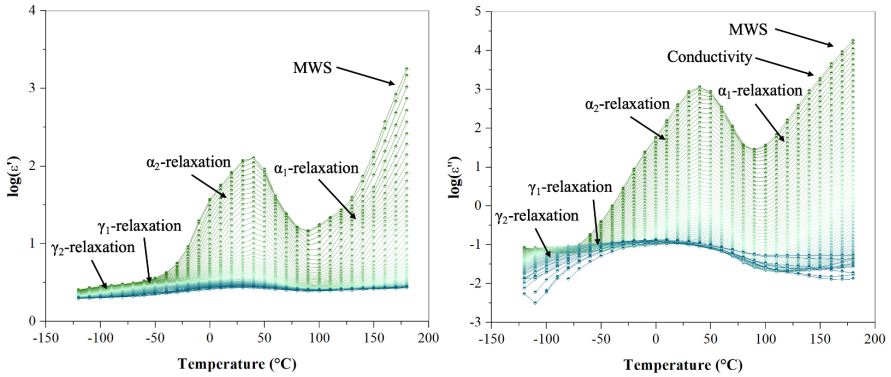


(a) LCNF-0h

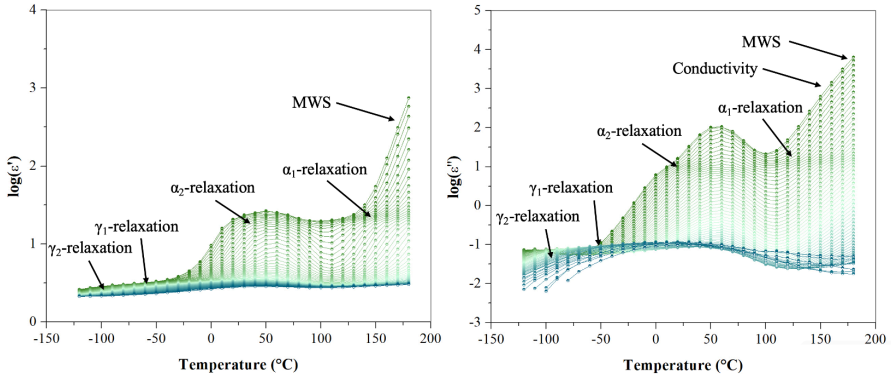


(b) LCNF-1h

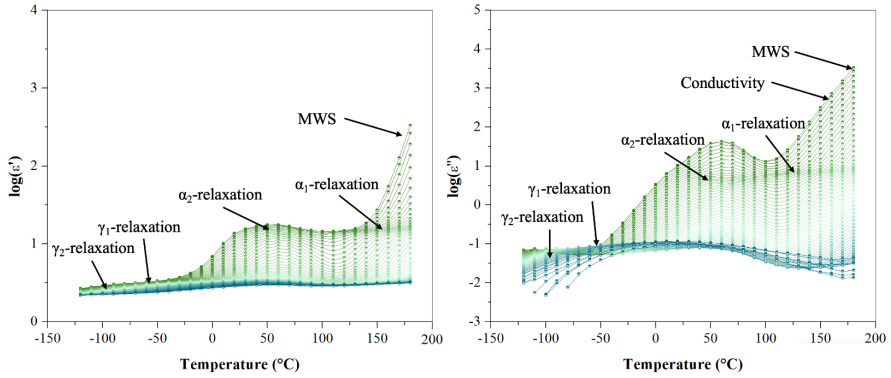


(c) LCNF-3h

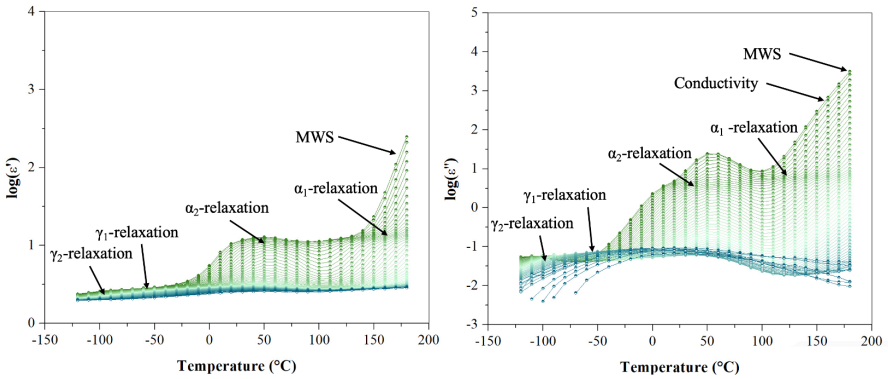


(d) LCNF-5h

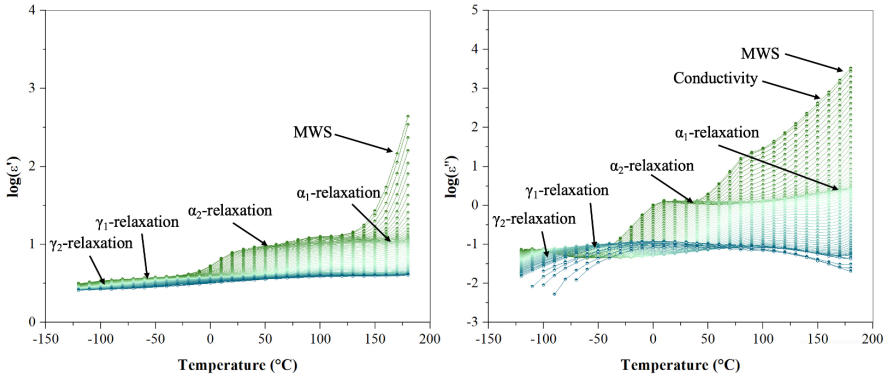


(e) LCNF-10h

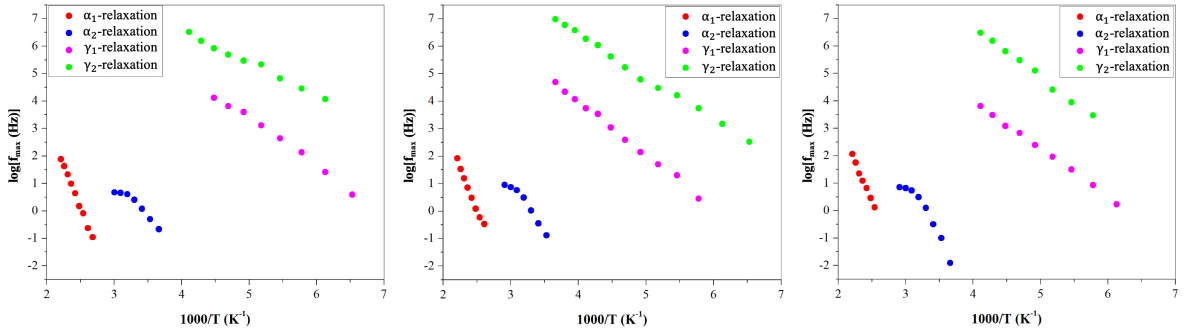


(f) LCNF-0h (g) LCNF-1h (h) LCNF-3h

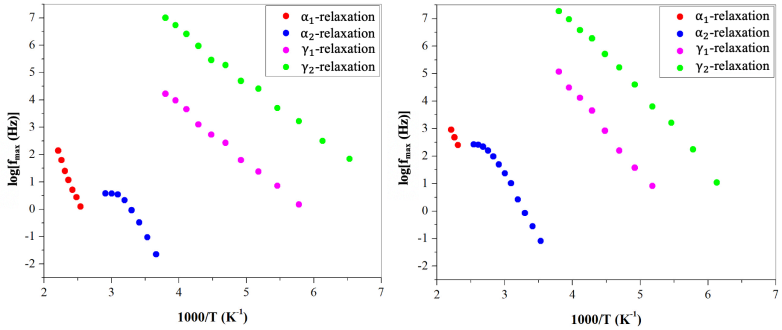


(i) LCNF-5h (j) LCNF-10h

**Figure 4.** (a-e) Dielectric spectra and (f-j) Arrhenius map of LCNFs from *Eucalyptus Nitens. The frequency range is* $10^{-2}$ *Hz to* $10^{7}$ *Hz.*

$\alpha_2$-relaxation shows a curvature at low frequencies, corresponding to a dynamic relaxation of the glass transition, associated with the motion of lignin. However, at low frequencies, this relaxation presents a linear zone (precursor relaxation), whose activation energy only decreases for LCNF-1h. This decrease may be due to the oxidation of lignin that generates a greater presence of polar groups, facilitating the motion of lignin segments.

The spectra show that ε' decreases with increasing reaction time ($\alpha_2$-relaxation, Figure 4a-e), due to the decrease in the amount of lignin and the increase in crosslinked structures in lignin that generate a lower capacity of the nanomaterial to store energy.

$\alpha_1$-relaxation can be associated with the moving segments of hemicellulose because the activation energy does not change with the content and oxidation of lignin, except for LCNF-10h where it decreases slightly. Hemicellulose plays an essential role in the surface properties of LCNFs, because LCNFs produced from hardwood have low proportions of xylans on the surface, leaving the cellulose exposed (Kumagai, 2018). This configuration indicates that the motions of the hemicellulose segments do not change (lignin-hemicellulose interactions), so the activation energy should be maintained. The slight decrease in the activation energy for LCNF-10h indicates that the oxidative process not only affected the cellulose, but also the hemicellulose.

**Table 5.** Activation energy (Ea) of relaxations in LCNFs from *Eucalyptus nitens*

| Sample | Relaxation | Ea (kJ/mol) | $R^2$ (%) |
|---|---|---|---|
| LCNF-0h | $\gamma_2$-relaxation | 22 | 99.2 |
| | $\gamma_1$-relaxation | 33 | 99.3 |
| | $\alpha_2$-relaxation[(a)] | 86 | 99.9 |
| | $\alpha_1$-relaxation | 118 | 99.7 |
| LCNF -1h | $\gamma_2$-relaxation | 30 | 99.6 |
| | $\gamma_1$-relaxation | 37 | 99.7 |
| | $\alpha_2$-relaxation[(a)] | 77 | 99.9 |
| | $\alpha_1$-relaxation | 115 | 99.2 |
| LCNF 3h | $\gamma_2$-relaxation | 36 | 99.6 |
| | $\gamma_1$-relaxation | 33 | 99.9 |
| | $\alpha_2$-relaxation[(a)] | 86 | 99.6 |
| | $\alpha_1$-relaxation | 111 | 99.4 |
| LCNF -5h | $\gamma_2$-relaxation | 36 | 99.7 |
| | $\gamma_1$-relaxation | 40 | 99.7 |
| | $\alpha_2$-relaxation[(a)] | 85 | 99.8 |
| | $\alpha_1$-relaxation | 116 | 99.4 |
| LCNF 10h | $\gamma_2$-relaxation | 51 | 99.6 |
| | $\gamma_1$-relaxation | 59 | 99.7 |
| | $\alpha_2$-relaxation[(a)] | 88 | 99.7 |
| | $\alpha_1$-relaxation | 105 | 99.9 |

[(a)] Linear zone of relaxation

To study the curved part of $\alpha_2$-relaxation in the Arrhenius map (Figure 4), the VFTH equation was used, whose parameters are shown in Table 6. Topological freezing temperatures or Vogel temperatures ($T_v$) follow the same trend as glass transition temperatures by DSC. When comparing the Tg by DSC and DETA ($T_v$+50K (Teruel-Juanes, 2020)), differences of lower than 12% were obtained. This allows corroborates that the glass transition obtained by DETA corresponds to the motion of lignin (Sixta, 2006; Heiner, 2019).

**Table 6.** Vogel-Fulcher-Tammann-Hesse parameters of the glass transition relaxation of lignin ($\alpha_2$-relaxation, curved zone).

| Sample | log[$\tau_0$ (Hz)] | $T_v$(K) | $T_g$[(a)] (K) | $D_0$ | $\Phi_g$/B | $\alpha_f$ x $10^4$ ($K^{-1}$) | Adjusted $R^2$ |
|---|---|---|---|---|---|---|---|
| LCNF-0h | 0.723±0.014 | 297.6±0.7 | 347.6 | 0.014±0.003 | 12.274 | 2454.9 | 1.0 |
| LCNF -1h | 1.341±0.086 | 286.3±2.6 | 336.3 | 0.179±0.042 | 0.911 | 195.3 | 1.0 |
| LCNF -3h | 0.977±0.030 | 303.3±1.5 | 353.3 | 0.038±0.009 | 4.391 | 878.2 | 1.0 |
| LCNF -5h | 0.786±0.102 | 291.6±3.8 | 341.6 | 0.074±0.037 | 2.330 | 466.1 | 0.97 |
| LCNF -10h | 2.657±0.095 | 333.9±6.0 | 383.9 | 0.090±0.044 | 1.664 | 332.7 | 0.98 |

[(a)] Tg calculated as $T_v$+50 K (Teruel-Juanes, 2020).

The values of log[$\tau_0$ (Hz)] do not follow a clear trend for these nanomaterials. On the other hand, $D_0$ values show that lignin oxidation produced an increase in the degree of deviation from the Arrhenius type temperature dependence, decreasing its brittleness. Furthermore, the increase in crosslinking in lignin produces a decrease in its brittleness.

The free volume coefficient ($\Phi$g/B) and expansion coefficient ($\alpha_f$) decreased with lignin oxidation, indicating an increase in crosslinking in lignin. However, an increase is observed for LCNF-3h, due to the high degree of delignification that removes part of the crosslinked structures. On the other hand, the low-value $\Phi$g/B for LCNF-1h could be influenced by the pronounced curvature in the $\alpha_2$-relaxation, which implied the use of limited points for the adjustment of the VFTH equation.

## 4. Conclusions

The oxidation with sodium chlorite did not affect the characteristics of the Eucalyptus *nitens* fibers, except for the 10 h of reaction time that generated an increase in crystallinity due to oxidative cleavage of the amorphous zone of the cellulose. The residual lignin from the oxidative processes in LCNFs presented a lower amount of β-O-4 ether bonds, fewer aliphatic and phenolic hydroxyl groups, and more ester, ketone, and carboxylic acid groups than native lignin. These chemical differences contribute to changes in the properties of the nanomaterial.

A lower amount of lignin favored longitudinal disintegration and hindered transverse disintegration of the fibers during mechanical pretreatment. This difference indicated an increase in selectivity in the fiber disintegration process for this species. On the other hand, the homogenization process was not affected by the content and oxidation degree of lignin. Therefore, a higher amount of lignin hindered the LCNF production process.

Fibrils of smaller width and more homogeneous width distribution were produced for LCNFs with a lower amount of lignin. However, the average apparent lengths increased, with no change in the distribution heterogeneity, independent of the degree of oxidation and content of lignin.

Regarding the rheological characteristics of LCNFs, the critical concentration decreased, and the viscosity increased for LCNFs with lower lignin content, due to the increase in flexibility, size, specific surface area, and surface charge of the fibrils.

A decrease in lignin content in *Eucalyptus nitens* pulps produced fibrils with larger morphologies and lower viscosities than *Pinus radiata* LCNFs, with similar ζ-potentials and degrees of delignification.

The LCNFs presented four dielectric relaxations associated with the molecular motions of cellulose, hemicellulose, and lignin and the motion of lignin and hemicellulose segments. The glass transition temperature of lignin showed two trends: a decrease caused by the molecular weight decrease, and an increase due to the rise in crosslinked structures.

## Ethics approval and consent to participate

Not applicable

## Consent for publication

Not applicable

## Availability of data and materials

Not applicable

## Competing interests

The authors have no relevant financial or non-financial interests to disclose.


## Funding

This work was funded by the Agencia Nacional de Investigación y Desarrollo (ANID)/Doctorado Nacional/2018–21181080, and projects FONDECYT N°1201042 and INNOMAT-H2 (MFA/2022/041) (Conselleria d'Innovació, Universitats, Ciència i Societat Digital).


## Authors' contributions

**Gregory Albornoz-Palma:** Conceptualization, Methodology, Validation, Formal analysis, Investigation, Writing – Original Draft; **Isidora Ortega-Sanhueza:** Investigation; **Roberto Teruel-Juanes:** Methodology, Validation, Investigation; **Sergio Henríquez-Gallegos:** Investigation, Writing – Review & Editing; **Amparo Ribes-Greus:** Conceptualization, Validation, Resources, Writing – Review & Editing, Supervision; **Miguel Pereira:** Conceptualization, Validation, Resources, Writing – Review & Editing, Supervision, Funding acquisition.


## Acknowledgments

We thank the Laboratorio de Biomateriales, Laboratorio de Análisis de Superficie y su Interacción con Fluidos (ASIF) (Departamento de Ingeniería Química, Universidad de Concepción).


## Authors' information (optional)


**Corresponding authors**

E-mail: gralbornoz@udec.cl. Phone: +56412661169.


## Reference


Agrebi F, Ghorbel N, Rashid B, et al (2018) Influence of treatments on the dielectric properties of sugar palm fiber reinforced phenolic composites. J Mol Liq 263:342–348. https://doi.org/10.1016/j.molliq.2018.04.130

Ahlgren PA, Goring DAI (1971) Removal of wood components during chlorite delignification of black spruce. Can J Chem 49:1272–1275. https://doi.org/10.1139/v71-207

633 Albornoz-Palma G, Betancourt F, Mendonça RT, et al (2020a) Relationship between rheological and
634 morphological characteristics of cellulose nanofibrils in dilute dispersions. Carbohydr Polym
635 230:115588. https://doi.org/10.1016/j.carbpol.2019.115588
636
637 Albornoz-Palma G, Ching D, Valerio O, et al (2020b) Effect of lignin and hemicellulose on the
638 properties of lignocellulose nanofibril suspensions. Cellulose 27:10631–10647.
639 https://doi.org/10.1007/s10570-020-03304-5
640
641 Albornoz-Palma G, Ching D, Henríquez-Gallegos S, et al (2022) The role of lignin in the production
642 process and characterization of lignocellulose nanofibril suspensions. Cellulose 29:8637–
643 8650. https://doi.org/10.1007/s10570-022-04791-4
644
645 Andrade A, Henríquez-Gallegos S, Albornoz-Palma G, Pereira M (2021) Effect of the chemical and
646 structural characteristics of pulps of Eucalyptus and Pinus on the deconstruction of the cell
647 wall during the production of cellulose nanofibrils. Cellulose 28:5387–5399.
648 https://doi.org/10.1007/s10570-021-03848-0
649
650 Ansari F, Berglund LA (2016) Tensile properties of wood cellulose nanopaper and nanocomposite
651 films. In: Multifunctional Polymeric Nanocomposites Based on Cellulosic Reinforcements.
652 Elsevier, pp 115–130
653
654 Antes R, Joutsimo OP (2014) Effect of Modified Cooking on Chemical Composition of Pulps from
655 Eucalyptus globulus and Eucalyptus nitens. Bioresources 10:.
656 https://doi.org/10.15376/biores.10.1.210-226
657
658 Awal A, Sain M (2011) Spectroscopic studies and evaluation of thermorheological properties of
659 softwood and hardwood lignin. J Appl Polym Sci 122:956–963.
660 https://doi.org/10.1002/app.34211
661
662 Back E., Salmen N (1982) Glass transitions of wood components hold implications for molding and
663 pulping processes. Tappi 65 (7): 107-110.
664
665 Badia JD, Teruel-Juanes R, Echegoyen Y, et al (2021) Effect of graphene nanoplatelets on the
666 dielectric permittivity and segmental motions of electrospun poly(ethylene-co-vinyl alcohol)
667 nanofibers. Polym Degrad Stab 183:109404.
668 https://doi.org/10.1016/j.polymdegradstab.2020.109404
669
670 Bastida GA, Schnell CN, Mocchiutti P, et al (2022) Effect of oxalic acid concentration and different
671 mechanical pre-treatments on the production of cellulose micro/nanofibers. Nanomaterials
672 (Basel) 12:2908. https://doi.org/10.3390/nano12172908
673
674 Ben H, Chen X, Han G, et al (2018) Characterization of whole biomasses in pyridine based ionic
675 liquid at low temperature by 31P NMR: An approach to quantitatively measure hydroxyl
676 groups in biomass as their original structures. Front Energy Res 6:.
677 https://doi.org/10.3389/fenrg.2018.00013
678
679 Bian H, Chen L, Dai H, Zhu JY (2017) Integrated production of lignin containing cellulose
680 nanocrystals (LCNC) and nanofibrils (LCNF) using an easily recyclable di-carboxylic acid.
681 Carbohydr Polym 167:167–176. https://doi.org/10.1016/j.carbpol.2017.03.050
682

683 Brebu M, Vasile C (2010) Thermal degradation of lignin—a review. *Cellulose Chemistry &*
684 *Technology*, *44*.9:353.
685
686 Börcsök Z, Pásztory Z (2020) The role of lignin in wood working processes using elevated
687 temperatures: an abbreviated literature survey. Eur J Wood Wood Prod.
688 https://doi.org/10.1007/s00107-020-01637-3
689
690 Budnikov D, Vasilev A, Vasilev A (2020) Studying of the dielectric loss factor of grain by indirect
691 method. E3S Web Conf 210:05002. https://doi.org/10.1051/e3sconf/202021005002
692
693 Cao W, Li J, Martí-Rosselló T, Zhang X (2019) Experimental study on the ignition characteristics of
694 cellulose, hemicellulose, lignin and their mixtures. J Energy Inst 92:1303–1312.
695 https://doi.org/10.1016/j.joei.2018.10.004
696
697 Carvalho DM de, Moser C, Lindström ME, Sevastyanova O (2019) Impact of the chemical
698 composition of cellulosic materials on the nanofibrillation process and nanopaper properties.
699 Ind Crops Prod 127:203–211. https://doi.org/10.1016/j.indcrop.2018.10.052
700
701 Chakraborty A, Sain M, Kortschot M (2006) Reinforcing potential of wood pulp-derived microfibres
702 in a PVA matrix. Holzforschung 60:53–58. https://doi.org/10.1515/hf.2006.010
703
704 Charlesworth JM (1993) Deconvolution of overlapping relaxations in dynamic mechanical spectra. J
705 Mater Sci 28:399–404. https://doi.org/10.1007/bf00357816
706
707 Chen Y, Fan D, Han Y, et al (2018) Effect of high residual lignin on the properties of cellulose
708 nanofibrils/films. Cellulose 25:6421–6431. https://doi.org/10.1007/s10570-018-2006-x
709
710 Chinga-Carrasco G (2011) Cellulose fibres, nanofibrils and microfibrils: The morphological sequence
711 of MFC components from a plant physiology and fibre technology point of view. Nanoscale
712 Res Lett 6:417. https://doi.org/10.1186/1556-276X-6-417
713
714 Collings GF, Yokoyama MT, Bergen WG (1978) Lignin as determined by oxidation with sodium
715 chlorite and a comparison with permanganate lignin. J Dairy Sci 61:1156–1160.
716 https://doi.org/10.3168/jds.s0022-0302(78)83700-x
717
718 Costa ALR, Gomes A, Tibolla H, et al (2018) Cellulose nanofibers from banana peels as a Pickering
719 emulsifier: High-energy emulsification processes. Carbohydr Polym 194:122–131.
720 https://doi.org/10.1016/j.carbpol.2018.04.001
721
722 Dorez G, Ferry L, Sonnier R, et al (2014) Effect of cellulose, hemicellulose and lignin contents on
723 pyrolysis and combustion of natural fibers. J Anal Appl Pyrolysis 107:323–331.
724 https://doi.org/10.1016/j.jaap.2014.03.017
725
726 Ek M, Gellerstedt G, Henriksson G (eds) (2009) Wood chemistry and wood biotechnology. Walter
727 de Gruyter
728
729 Fulcher GS (1925) Analysis of recent measurements of the viscosity of glasses. J Am Ceram Soc
730 8:339–355. https://doi.org/10.1111/j.1151-2916.1925.tb16731.x
731

Gindl-Altmutter W, Obersriebnig M, Veigel S, Liebner F (2015) Compatibility between cellulose and hydrophobic polymer provided by microfibrillated lignocellulose. ChemSusChem 8:87–91. https://doi.org/10.1002/cssc.201402742

Gu L, Jiang B, Song J, et al (2019) Effect of lignin on performance of lignocellulose nanofibrils for durable superhydrophobic surface. Cellulose 26:933–944. https://doi.org/10.1007/s10570-018-2129-0

Havriliak S, Negami S (2007) A complex plane analysis of α-dispersions in some polymer systems. J Polym Sci C Polym Symp 14:99–117. https://doi.org/10.1002/polc.5070140111

Havriliak S, Negami S (1967) A complex plane representation of dielectric and mechanical relaxation processes in some polymers. Polymer (Guildf) 8:161–210. https://doi.org/10.1016/0032-3861(67)90021-3

Heitner C, Dimmel D, Schmidt J (eds) (2016) Lignin and Lignans: Advances in Chemistry. CRC Press, Boca Raton, FL

Hergert HL (1960) Infrared spectra of lignin and related compounds. II. Conifer lignin and model Compounds1,2. J Org Chem 25:405–413. https://doi.org/10.1021/jo01073a026

Iglesias MC, Shivyari N, Norris A, et al (2020) The effect of residual lignin on the rheological properties of cellulose nanofibril suspensions. J Wood Chem Technol 40:370–381. https://doi.org/10.1080/02773813.2020.1828472

Ioelovich M (2016) Isophase Transitions of Cellulose – A Short Review. Athens J Sci 3:309–322. https://doi.org/10.30958/ajs.3-4-4

ISO, ISO/TS 20477:2017 Nanotechnologies – Standard terms and their definition for cellulose nanomaterial, ISO, Geneva, Switzerland, 2017.

Iwamoto S, Abe K, Yano H (2008) The effect of hemicelluloses on wood pulp nanofibrillation and nanofiber network characteristics. Biomacromolecules 9:1022–1026. https://doi.org/10.1021/bm701157n

Iwamoto S, Lee S-H, Endo T (2014) Relationship between aspect ratio and suspension viscosity of wood cellulose nanofibers. Polym J 46:73–76. https://doi.org/10.1038/pj.2013.64

Jang J-H, Hayashi N, Han S-Y, et al (2020) Changes in the dimensions of lignocellulose nanofibrils with different lignin contents by enzymatic hydrolysis. Polymers (Basel) 12:2201. https://doi.org/10.3390/polym12102201

Jiang Y, Liu X, Yang Q, et al (2018) Effects of residual lignin on mechanical defibrillation process of cellulosic fiber for producing lignocellulose nanofibrils. Cellulose 25:6479–6494. https://doi.org/10.1007/s10570-018-2042-6

Jones RG, Kahovec J, Stepto R, et al (eds) (2009) Appendix: Bibliography of biopolymer-related IUPAC-IUBMB nomenclature recommendations. In: Compendium of Polymer Terminology and Nomenclature. Royal Society of Chemistry, Cambridge, pp 408–409.

Kolar JJ, Lindgren BO, Pettersson B (1983) Chemical reactions in chlorine dioxide stages of pulp bleaching: Intermediately formed hypochlorous acid. Wood Sci Technol 17:117–128. https://doi.org/10.1007/bf00369129

Kremer F, Schonhals A (eds) (2012) Broadband dielectric spectroscopy. Springer, Berlin, Germany.

Kumagai A, Endo T (2018) Comparison of the surface constitutions of hemicelluloses on lignocellulosic nanofibers prepared from softwood and hardwood. Cellulose 25:3885–3897. https://doi.org/10.1007/s10570-018-1861-9

Larson RG, Wei Y (2019) A review of thixotropy and its rheological modeling. J Rheol (N Y N Y) 63:477–501. https://doi.org/10.1122/1.5055031

Lee J-A, Yoon M-J, Lee E-S, et al (2014) Preparation and characterization of cellulose nanofibers (CNFs) from microcrystalline cellulose (MCC) and CNF/polyamide 6 composites. Macromol Res 22:738–745. https://doi.org/10.1007/s13233-014-2121-y

Lehto J, Louhelainen J, Kłosińska T, et al (2018) Characterization of alkali-extracted wood by FTIR-ATR spectroscopy. Biomass Convers Biorefin 8:847–855. https://doi.org/10.1007/s13399-018-0327-5

Lekha P, Mtibe A, Motaung, T, Andrew J, Sitholè, B, Gibril M (2016) Effect of mechanical treatment on properties of cellulose nanofibrils produced from bleached hardwood and softwood pulps. Maderas. Ciencia y tecnología, 18(3), 457-466. http://dx.doi.org/10.4067/S0718-221X2016005000041

Lemeune S, Jameel H, Chang H-M, Kadla JF (2004) Effects of ozone and chlorine dioxide on the chemical properties of cellulose fibers. J Appl Polym Sci 93:1219–1223. https://doi.org/10.1002/app.20509

Li Y, Fu Q, Yang X, Berglund L (2018) Transparent wood for functional and structural applications. Philos Trans A Math Phys Eng Sci 376:20170182. https://doi.org/10.1098/rsta.2017.0182

Lisperguer J, Perez P, Urizar S (2009) Structure and thermal properties of lignins: characterization by infrared spectroscopy and differential scanning calorimetry. J Chil Chem Soc 54(4), 460-463. http://dx.doi.org/10.4067/S0717-97072009000400030.

Liu Y, Chen B, Lv Y, et al (2022) Insight into the performance of lignin-containing cellulose nanofibers (LCNFs) via lignin content regulation by p-toluenesulfonic acid delignification. Cellulose 29:2273–2287. https://doi.org/10.1007/s10570-022-04432-w

Ma Q, Zhu J, Gleisner R, et al (2018) Valorization of wheat straw using a recyclable hydrotrope at low temperatures (≤90 °C). ACS Sustain Chem Eng 6:14480–14489. https://doi.org/10.1021/acssuschemeng.8b03135

Malešič J, Kraševec I, Kralj Cigić I (2021) Determination of cellulose degree of polymerization in historical papers with high lignin content. Polymers (Basel) 13:1990. https://doi.org/10.3390/polym13121990

Mansfield ML, Douglas JF (2008) Transport properties of wormlike chains with applications to double helical DNA and carbon nanotubes. Macromolecules 41:5412–5421. https://doi.org/10.1021/ma702837v

Meng X, Pu Y, Sannigrahi P, et al (2018) The nature of hololignin. ACS Sustain Chem Eng 6:957–964. https://doi.org/10.1021/acssuschemeng.7b03285

Morais FP, Bértolo RAC, Curto JMR, et al (2019) Comparative characterization of eucalyptus fibers and softwood fibers for tissue papers applications. Materials Letters: X 4:100028. https://doi.org/10.1016/j.mlblux.2019.100028

Muraleedharan MN, Zouraris D, Karantonis A, et al (2018) Effect of lignin fractions isolated from different biomass sources on cellulose oxidation by fungal lytic polysaccharide monooxygenases. Biotechnol Biofuels 11:296. https://doi.org/10.1186/s13068-018-1294-6

Murali Krishnan J, Deshpande Abhijit P, Sunil Kumar PB (eds) (2010) Rheology of complex fluids. Springer, New York, NY.

Nair SS, Sharma S, Pu Y, et al (2014) High shear homogenization of lignin to nanolignin and thermal stability of nanolignin-polyvinyl alcohol blends. ChemSusChem 7:3513–3520. https://doi.org/10.1002/cssc.201402314

Nazari B, Kumar V, Bousfield DW, Toivakka M (2016) Rheology of cellulose nanofibers suspensions: Boundary driven flow. J Rheol (N Y N Y) 60:1151–1159. https://doi.org/10.1122/1.4960336

Nechyporchuk O, Belgacem MN, Pignon F (2016) Current progress in rheology of cellulose nanofibril suspensions. Biomacromolecules 17:2311–2320. https://doi.org/10.1021/acs.biomac.6b00668

Nunes CA, Lima CF, Barbosa LCA, et al (2010) Determination of Eucalyptus spp lignin S/G ratio: a comparison between methods. Bioresour Technol 101:4056–4061. https://doi.org/10.1016/j.biortech.2010.01.012

Ochoa-Villarreal M, Aispuro-Hernndez E, Vargas-Arispuro I, Ngel M (2012) Plant cell wall polymers: Function, structure and biological activity of their derivatives. In: Polymerization. InTech

Pejic BM, Kostic MM, Skundric PD, Praskalo JZ (2008) The effects of hemicelluloses and lignin removal on water uptake behavior of hemp fibers. Bioresour Technol 99:7152–7159. https://doi.org/10.1016/j.biortech.2007.12.073

Rencoret J, Gutiérrez A, del Río JC (2007) Lipid and lignin composition of woods from different eucalypt species. Holzforschung 61:165–174. https://doi.org/10.1515/hf.2007.030

Ribes, A. (1986). Relajaciones dieléctricas y viscoelásticas en los polietilenos de alta y baja densidad. Tesis Doctoral. Universitat de València, España.

Roig F, Ramanantsizehena G, Lahatra Razafindramisa F, et al (2017) Dielectric and mechanical properties of various species of Madagascan woods. Wood Sci Technol 51:1389–1404. https://doi.org/10.1007/s00226-017-0936-3

Segal L, Creely JJ, Martin AE Jr, Conrad CM (1959) An empirical method for estimating the degree of crystallinity of native cellulose using the X-ray diffractometer. Text Res J 29:786–794. https://doi.org/10.1177/004051755902901003

Sixta H (eds) (2006) Handbook of paper and board. John Wiley & Sons.

Stark NM, Yelle DJ, Agarwal UP (2016) Techniques for Characterizing Lignin. In: Lignin in Polymer Composites. Elsevier, pp 49–66

Sun N, Das S, Frazier CE (2007) Dynamic mechanical analysis of dry wood: Linear viscoelastic response region and effects of minor moisture changes. Holzforschung 61:28–33. https://doi.org/10.1515/hf.2007.006

Tarvo V, Lehtimaa T, Kuitunen S, et al (2010) A model for chlorine dioxide delignification of chemical pulp. J Wood Chem Technol 30:230–268. https://doi.org/10.1080/02773810903461476

Teruel-Juanes R, Pascual-Jose B, del Río C, et al (2020) Dielectric analysis of photocrosslinked and post-sulfonated styrene-ethylene-butylene-styrene block copolymer based membranes. React Funct Polym 155:104715. https://doi.org/10.1016/j.reactfunctpolym.2020.104715

Torgovnikov GI (1993) Dielectric properties of wood-based materials. In: Dielectric Properties of Wood and Wood-Based Materials. Springer Berlin Heidelberg, Berlin, Heidelberg, pp 135–159

Vural D, Gainaru C, O'Neill H, et al (2018) Impact of hydration and temperature history on the structure and dynamics of lignin. Green Chem 20:1602–1611. https://doi.org/10.1039/c7gc03796a

Wentzel M, Fleckenstein M, Hofmann T, Militz H (2019) Relation of chemical and mechanical properties of Eucalyptus nitens wood thermally modified in open and closed systems. Wood Mater Sci Eng 14:165–173. https://doi.org/10.1080/17480272.2018.1450783

Yang H, Yan R, Chen H, et al (2007) Characteristics of hemicellulose, cellulose and lignin pyrolysis. Fuel (Lond) 86:1781–1788. https://doi.org/10.1016/j.fuel.2006.12.013

Yuan T, Zeng J, Wang B, et al (2021) Lignin containing cellulose nanofibers (LCNFs): Lignin content-morphology-rheology relationships. Carbohydr Polym 254:117441. https://doi.org/10.1016/j.carbpol.2020.117441

Zeng X, Deng L, Yao Y, et al (2016) Flexible dielectric papers based on biodegradable cellulose nanofibers and carbon nanotubes for dielectric energy storage. J Mater Chem C Mater Opt Electron Devices 4:6037–6044. https://doi.org/10.1039/c6tc01501h

Zhang J, Choi YS, Yoo CG, et al (2015) Cellulose–Hemicellulose and Cellulose–Lignin Interactions during Fast Pyrolysis. ACS Sustain Chem Eng 3:293–301. https://doi.org/10.1021/sc500664h